What first principles molecular dynamics can tell us about EXAFS spectroscopy of radioactive heavy metal cations in water

By M. Duvail[1], P. D'Angelo[2], M.-P. Gaigeot[1], P. Vitorge[1,3] and R. Spezia[1,*]

[1] Laboratoire Analyse et Modélisation pour la Biologie et l'Environnement, UMR 8587 CNRS, Université d'Evry Val d'Essonne, 91025 Evry Cedex, France
[2] Dipartimento di Chimica, Università di Roma La Sapienza, 00185 Roma, Italy
[3] Laboratoire de Spéciation des Radionucléides et Molécules, CEA Saclay, DEN/DPC/SECR, 91191 Gif-sur-Yvette, France

Summary. In this paper we show how molecular dynamics simulation can improve comprehension of structure and dynamics of water solvent around heavy cations. In particular, metal-water radial distribution function obtained from molecular dynamics can be used into EXAFS equation to improve the experimental signal fitting. Here we show results on structure and dynamics of Co^{2+}, that is a radiocontaminant cation in its isotopic form ^{60}Co, and lanthanoids(III) that are the chemical analogues of actinides(III) in aqueous solution.

1. Introduction

The comprehension of heavy metal cations hydration is a basic step to rationalize from microscopic point of view their role in aqueous environment, like in industrial and nuclear circuits and in geological media. Different experimental and theoretical approaches were developed and used in last years to address the fundamental question of understanding structure and dynamics of water molecules around ions [1–5]. From an experimental point of view neutron and X-ray diffraction and X-ray absorption are the techniques of choice. Theoretically two kind of approaches can be identified: (i) geometry optimization methods that lead to the minimum energy of a finite system where the cation is surrounded by a limited number of water molecules [5–9] (generally one or two shells are treated and sometimes a continuum is added to mimic the solvation field); (ii) finite temperature molecular dynamics that is devoted to sample phase space of a system with a huge number of degrees of freedom, that is applied to mimic bulk systems [10–15]. The key point, common for both theoretical approaches, is the description of metal-water and water-water interactions, since results will be strongly dependent on that. Quantum chemistry can be used at this aim. To obtain the structure of minimum energy (used generally for isolated clusters) relatively high level calculations can be performed. Of course, when interested in radioactive heavy elements

we have to deal with elements bearing a huge number of electrons, so that highly-correlated methods and relativistic effects must be taken into account. This last effect is generally implicitly considered by using pseudo-potentials so that core electrons are not explicitly treated [16, 17]. For molecular dynamics simulations, at the present time, it is computationally impossible to use high level theoretical calculations. A first possible approach is to use classical interaction potentials, such that systems composed by thousands of atoms for a time length of ns-μs can be actually simulated. This means that metal-water and water-water interactions are modelled *via* analytical potentials whose parameters are obtained to reproduce either macroscopic experimental properties or *ab initio* structure [18–20]. Recently, Car-Parrinello DFT-based molecular dynamics have taken a place of choice in the panorama of MD methods to simulate metals in presence of bulk water for a time length of some picoseconds [21–30]. This means that the parameterization procedure is not needed but only very fast processes can be studied and, for example, it is difficult (if not impossible) to study exchange reactions of water molecules in the first solvation shell.

Molecular dynamics has the advantage to provide structure and dynamics of water molecules around the first hydration shell at finite temperature. Results can be compared with different kind of experiments, but recently a particular interest was focused on the coupling with EXAFS spectroscopy [31–39]. In particular, metal-water distance and dynamics obtained from MD simulations can be directly related to EXAFS data, notably scattering paths and Debye–Waller factors [40, 41]. In the MD approach presented in this work, based on the resolution of classical Newton's equation of motion for nuclei, only structural parameters can be addressed from calculations. Non-structural parameters related to the absorption of the X-ray radiation from a core electron and the successive photoemission process need a different theoretical approach, that is beyond our aim in the present paper. Thus, here we show how molecular dynamics of Co^{2+}, La^{3+} and Lanthanide tri-cations (Ln^{3+}) series can provide reliable information on hydration structure and dynamics and help in interpreting EXAFS experiments.

In the present paper we show two examples of heavy metals: (i) hydration of Co^{2+}, that in its ^{60}Co isotopic form

* Author for correspondence
(E-mail: riccardo.spezia@univ-evry.fr).

is an important radioactive contaminant, is treated by DFT-based MD since d electrons play an important role in defining complaxation; (ii) hydration of La^{3+} and Ln^{3+}, that are chemical analogues of actinides. We present here two systems with different first hydration shell coordination number (CN) – six for Co^{2+}, nine for La^{3+} and light lanthanides and eight for heavy lanthanides – and consequently different geometries. These cations present also radioactive isotopes. ^{60}Co is an activation product produced in water circuits of nuclear power plants. It has an important contribution to the exposure of the workers of this industry. Light lanthanides are fission products. For waste management studies – specially assessments of the environmental impacts of future geological waste disposals – lanthanides are also used as chemical analogues to predict the geochemical behaviours of Am and Cm, and Pu(III) in reducing conditions as typically in deep ground-waters.

The reminder of the paper is as follows: in the first section we will describe the theoretical methods employed for molecular dynamics and for obtaining EXAFS signal from MD results. Than we show how MD and EXAFS results can be directly coupled for Co^{2+} and La^{3+} hydration and then we present results for the whole Ln series. General conclusions end the present contribution.

2. Methods

2.1 Molecular dynamics

We performed Car-Parrinello molecular dynamics (CPMD) to study Co^{2+} hydration. The metal was immersed in 64 water molecules, using a cubic box of 12.42 Å to reproduce water density at 300 K. Periodic boundary conditions were applied to mimic bulk system using Ewald summation for long range interactions. Simulations were performed with the CPMD package [42, 43] in the NVE ensemble. The system was initially equilibrated at 300 K generating initial velocities from a Maxwell distribution centered at the target temperature and then performing 1 ps of MD equilibration. CPMD data were then collected over 5 ps of simulation, without control of the temperature. A fictitious mass of 400 au was used and a time step of 4 au (0.097 fs) was employed to numerically solve motion equations. The electronic structure of valence electrons was expanded in plane waves with an energy cutoff of 90 Ry. Medium soft norm-conserving pseudopotentials of the Trouillier–Martins type [44] were used. Standard Trouillier–Martins pseudopotentials of O and H atoms were used. Co^{2+} was considered in the quartet state, corresponding to the experimental spin state [45, 46]. The Co^{2+} pseudopotential retains only the $3d^7$ and $4s^0$ electronic levels as valence states. Other details on the Co pseudopotential are reported elsewhere [47]. Energy expectations were calculated in reciprocal space using the Kleinman–Bylander transformation [48]. Nonlinear core corrections [49] – that are recommended for transition metals – were applied with a core-charge radius of 1.2 Bohr.

For studying lanthanide hydration, where water exchanges can occur in a timescale of hundreds picoseconds, classical molecular dynamics (CLMD) was employed. Ln^{3+} ions were immersed in box containing 216 water molecules.

We employed periodic boundary conditions with Ewald summation for long range interactions. Simulations were done at room temperature, generating velocities at 300 K and thus performing equilibration MD at the target temperature to equilibrate the system. Then, NVE simulations were performed for 3 ns. Also in this case room temperature was maintained through the simulations.

Ln^{3+}-water and water-water interactions were treated using a pair potential where polarization effects were added in the electrostatic term (V_{elec})

$$V_{tot} = V_{elec} + V_{O-O}^{LJ} + V_{Ln-O}. \tag{1}$$

Water molecules were modelled *via* a modified rigid TIP3P model [20, 50] while Ln^{3+}-water non-electrostatic interactions (V_{Ln-O}) were modelled using the following analytical potential

$$V_{Ln-O}(r) = A\exp(-Br) - \frac{C}{r^6}, \tag{2}$$

where r is the Ln−O distance and A, B, C are three parameters that depend on the Ln element. These parameters were evaluated for La^{3+} fitting the potential of Eq. (2) over *ab initio* (at MP2 level) curves [20] and, since they are related to ionic radii and polarizabilities, they are extended to all the lanthanide series [51, 52]. Parameters used in this work are presented in Table 2 in conjunction with atomic properties considered. Polarizability was taken into account using the Thole's induced dipole model [53]. Atomic dipoles were calculated at the beginning by using a self-consistent procedure and then propagated by adding an associate dynamical variable and fictitious mass to the system Hamiltonian, as described by us in Ref. [20] and proposed by Sprik few years ago [54].

2.2 EXAFS signal

The relation between the EXAFS $\chi(k)$ signal and the local structure – defined through the n-body distribution functions – contains the integrals of the two-atom ($\gamma^{(2)}$), three-atom ($\gamma^{(3)}$) and n-atom ($\gamma^{(n)}$) signals, which can be calculated using the multiple-scattering (MS) theory [55]. In *conventional* EXAFS data analysis of disordered systems, only two-body distributions are considered, and the $\chi(k)$ signal is represented by the equation

$$\chi(k) = \int_0^\infty 4\pi\rho r^3 g(r) A(k,r) \sin[2kr + \phi(k,r)]\, dr,$$

$$\tag{3}$$

where $A(k,r)$ and $\phi(k,r)$ are the amplitude and phase functions, respectively, and ρ is the density of the scattering atoms and $g(r)$ is the radial distribution function (RDF). $\chi(k)$ theoretical signals can be calculated by introducing into Eq. (3) the model radial distribution functions obtained from CPMD or CLMD simulations of cations in bulk water. Both M−O and M−H $g(r)$ distributions obtained from simulations have been used to calculate the single scattering first shell $\chi(k)$ theoretical signal, because the ion-hydrogen interactions have been determined to provide a detectable

contribution to the EXAFS spectra of transition-metal ions in aqueous solutions [33, 56]. This should be of much importance for ions that coordinate nine or eight water molecules, such as lanthanides.

The EXAFS theoretical signals have been calculated by means of the GNXAS program. Phase shifts, $A(k, r)$ and $\phi(k, r)$, have been calculated using a reference geometry issued by MD using muffin-tin potentials and advanced models for the exchange-correlation self-energy (Hedin–Lundqvist) [57]. The values of muffin-tin radii are 0.3, 0.9, 1.2 and 1.7 Å for hydrogen, oxygen, cobalt and lanthanium, respectively. Inelastic losses of the photoelectron in the final state have been intrinsically accounted for by complex potential. The imaginary part also includes a constant factor accounting for the core-hole width [58].

Peak shapes of calculated RDF's (Co−O, Co−H, La−O and La−H) are modelled with gamma-like distribution curves with a mean distance R_m, a standard deviation σ, and asymmetry index β (the third cumulant divided by σ^3) $\beta = 2p^{-1/2}$ that can be gradually varied in a wide range. It is important to remind that, as for the Gaussian distribution, the dumping of the $\chi(k)$ signal averaged over the gamma distribution can be calculated exactly [31].

The EXAFS experimental spectrum of Co^{2+} in water collected at the EMBL at DESY above the K-edge. Measurements were performed at room temperature with a Si(220) double-crystal monochromator. The La^{3+} K-edge spectra were collected at ESRF, on the bending magnet X-ray absorption spectroscopy beam line BM29, [59] in transmission geometry. Details on experimental procedure are described elsewhere [60].

3. Results and discussion

3.1 Co^{2+} and La^{3+} hydrations

Co^{2+} and La^{3+} in water are known to form stable structures where the cation coordinate six and nine water molecules respectively. Co^{2+} forms an octahedral complex while La^{3+} forms a trigonal tricapped prism (TTP), as shown in Fig. 1. Solvation structural and dynamical properties obtained by CPMD and CLMD dynamics, for Co^{2+} and La^{3+} respectively, are shown in Table 1.

Liquid phase experiments provide a metal-oxygen distance of 2.09 Å for Co^{2+} and 2.54–2.56 Å for La^{3+} [33, 61, 62]. EXAFS experiments can add information on Debye–Waller factor that is a mesure of metal-ligand dy-
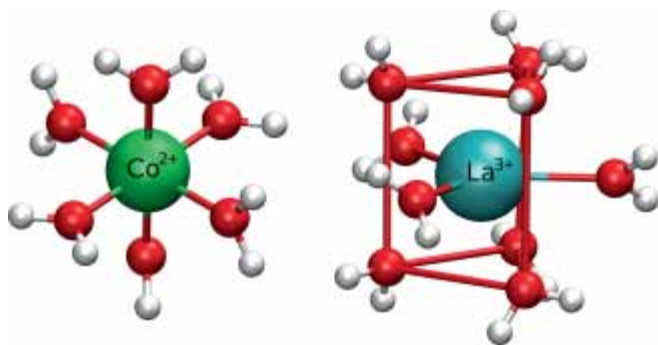
Table 1. Structural properties of Co^{2+} and La^{3+} solvation. $r^{(1)}$ and $r^{(2)}$ are the first and second peak of radial distribution function, respectively; CN is the coordination number. Exp are EXAFS experimental data.

	CLMD	CPMD	Exp
$r_{Co-O}^{(1)}$ (Å)	2.07^a	2.10	2.09^b
$CN_{Co-O}^{(1)}$	6^a	6	6.0^b
$r_{Co-H}^{(1)}$ (Å)	2.76^a	2.72	−
$CN_{Co-H}^{(1)}$	12^a	12	−
$r_{Co-O}^{(2)}$ (Å)	4.3^a	4.10	4.28^c
$CN_{Co-O}^{(2)}$	11.48^a	12.48	14.8^c
$r_{La-O}^{(1)}$ (Å)	2.52	−	2.54^d
$CN_{La-O}^{(1)}$	9.02	−	9.20^d
$r_{La-H}^{(1)}$ (Å)	3.17	−	−
$CN_{La-H}^{(1)}$	18.5	−	−
$r_{La-O}^{(2)}$ (Å)	4.65	−	4.63^e
$CN_{La-O}^{(2)}$ (Å)	18.8	−	18^e
$MRT_{La-O}^{(2)}$ (ps)	7.6	−	−

a: from Ref. [37]; b: from Ref. [33]; c: from Ref. [2]; d: from Ref. [61]; e: from Ref. [62].

namics. As described in the previous section, the structure of ligand around a metallic center can be fully described by the radial distribution function (RDF). Quite often a gaussian distribution is employed to model RDF's. This is a poor description in the case of structure in liquid phase, where anharmonicity and asymmetry play an important role. Thus, the gamma distribution, that is an asymmetric distribution, was used to describe metal-ligand – and photoabsorber-scattering atoms – interaction, as obtained from MD simulations and as they are fitted in an independent EXAFS data analysis. In Fig. 2, we show RDF obtained from MD simulations and from EXAFS data analysis. The peak position, that corresponds to single scattering path length, agrees relatively well between calculations and experiments, while a difference is found in distribution width (related to
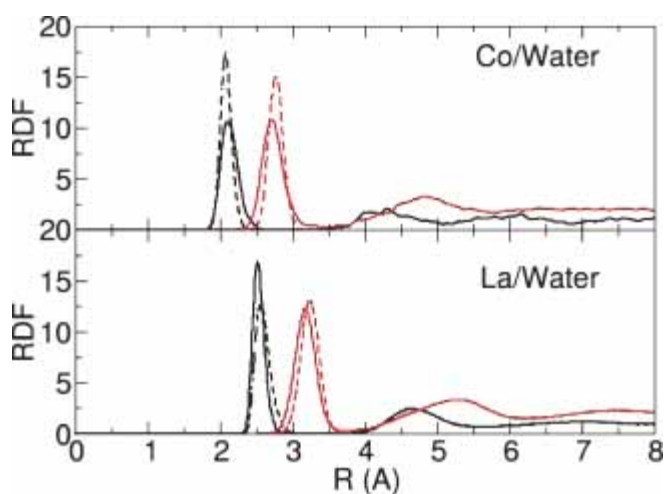

Fig. 1. $Co^{2+}(H_2O)_6$ and $La^{3+}(H_2O)_9$ first solvation shell structures.

Fig. 2. Co^{2+}-water and La^{3+}-water radial distribution functions, as obtained from CPMD and CLMD molecular dynamics (filled lines) for Co^{2+} and La^{3+} respectively and from EXAFS fitting (dashed lines). M−O RDF are in black, M−H in red, where M is Co for the upper panel and La for the lower one.

Table 2. Paremeters obtained fitting the first RDF peaks with a gamma distribution function compared with the equivalent parameters obtained from EXAFS fitting. Co-water EXAFS fitting parameters are taken from our previous work [37], while La-water ones are from the present work.

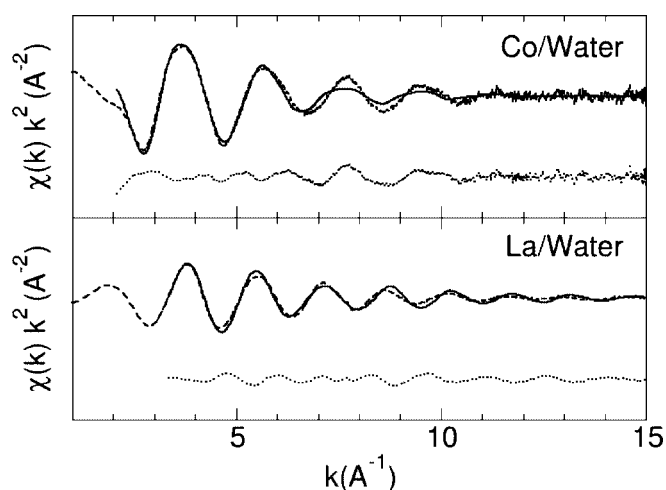|	R_m (Å)	σ^2 (Å²)	β	N
Co–O/CPMD	2.14	0.015	0.4	6
Co–O/EXAFS	2.092(2)[a]	0.0062(5)[a]	0.3 (1)[a]	6.0(1)[a]
Co–H/CPMD	2.75	0.021	0.4	12.5
Co–H/EXAFS	2.78 (2)[a]	0.010 (4)[a]	0.05(9)[a]	12.1(2)[a]
La–O/CLMD	2.54	0.0070	0.5	8.9
La–O/EXAFS	2.549(0.007)	0.0086(0.001)	0.7(0.1)	9.1(0.5)
La–H/CLMD	3.191	0.020	0.060	18.12
La–H/EXAFS	3.250(0.03)	0.011 (0.003)	1.4(0.6)	18.1(0.9)

a: from Ref. [37].

Fig. 3. EXAFS signal calculated using radial distribution functions from CPMD and CLMD simulations for hydrated Co^{2+} and La^{3+} respectively (filled lines). Experimental and residual signal are reported in dashed and dotted lines.

Table 3. Non structural parameters fitting EXAFS signals by using gamma distributions for M−O and M−X scattering paths.

	Co^{2+}_{aq}/ EXAFS	Co^{2+}_{aq}/ CPMD	La^{3+}_{aq}/ EXAFS	La^{3+}_{aq}/ CLMD
E_0 (eV)	7711	7722	38 940	38 935
S_0^2	0.99	0.98	0.99	0.99
E_1 (eV)	7752	7785	39 038	39 080
E_2 (eV)	7721	7843	39 170	39 165
E_3 (eV)	−	−	39 192	39 172
R	0.65×10^{-6}	0.71×10^{-6}	0.39×10^{-7}	0.11×10^{-5}

DW factors and asymmetry). In Table 2 we report parameters of photoabsorber-scattering atoms for Co^{2+} and La^{3+} as obtained from simulations (fitting RDFs obtained from molecular dyanamics simualtions with gamma distribution function) and experiments (assuming a gamma distribution of the corresponding single scattering path).

We should remark that the structural information are independently obtained and Eq. (2) is used to trace $\chi(k)k^2$ *vs.* k signal presented in Fig. 3 by using the $g(r)$ obtained from molecular dynamics simulations and only for non structural parameters we used in Eq. (2) those obtained from an independent EXAFS fitting. This was done with the aim of comparing theoretical results with experiments, leaving experimental fitting independent from simulations which reliability we want to investigate.

DW factors were found overestimated in CPMD with respect to experiments, while the opposite picture is obtained from CLMD simulations. The first results are quite expected, and noticed yet also for transition metal complexes [46], since DW factors are related to bond vibrations. CPMD simulations are known to reproduce well infra-red experiments (and thus vibrational frequencies) with a systematic red shift of about $100 \, cm^{-1}$, that roughly corresponds to the difference in DW factors. On the other hand,

CLMD simulations, that slightly underestimate La−O distance, provide smaller DW factors.

It is possible thus to fit the experimental EXAFS signal by using the M−O and M−H scattering paths (and associated σ^2 and β) as obtained from RDFs issued from simulations. RDF's are also here fitted by gamma distributions. In Fig. 3 we show the resulting $\chi(k)$ signals for Co^{2+} and La^{3+} in water. We should notice that in both cases, the theoretical signal agrees well with the experimental one, even if some differences are found in signal amplitude, for low k, and a dephasing is obseved at higher k values. Non structural parameters are summarized in Table 3, where the overall fitting quality is also reported.

3.2 Hydration structure of other lanthanides

Atoms in the Lanthanide series have the same charge ($+3$) of La when dissolved in water, forming aqua-complexes with coordination number (CN) of nine (like La) for the first atoms in the series and CN of 8 for the last ones. Across the series it is known that both ionic radius and polarizability have a linear behaviour, as reported in the literature [66, 67]. Using these known linear dependences we could extrapolate ionic radius and polarizability for Pm^{3+} that is the unique not natural atom in the series.

CLMD simulations were thus performed using the different atomic polarization for the electrostatic contribution of Ln-water interaction and modifying B and C parameters of Eq. (2) that account for non-electrostatic contributions in Ln-water interaction. The La−O parameters were modified for the other atoms in the series taking into account their relationship with atomic properties. In particular for B we

Table 4. Parameters (B and C), structural and dynamical results for hydration of Lanthanides. Experimental data are shown in parenthesis for comparison. B is in Å^{-1}, C in kJ mol^{-1}, r in Å and mean residence time (MRT) in ps. $r^{(I)}$, $\text{CN}^{(I)}$ and $\text{MRT}^{(I)}$ are results for first hydration shell, $R^{(II)}$, $\text{CN}^{(II)}$ and $\text{MRT}^{(II)}$ are for second hydration shell.

Atom	B	C	$r_{\text{LnO}}^{(I)}$ (Å)	$\text{CN}^{(I)}$	$\text{MRT}^{(I)}$	$r_{\text{LnO}}^{(II)}$ (Å)	$\text{CN}^{(II)}$	$\text{MRT}^{(II)}$
Ce	3.500	3.628×10^4	2.50 (2.538[a], 2.52[b], 2.53[c])	9.00 (9.3[b])	1769	4.65	19.3	6.6
Pr	3.517	3.535×10^4	2.49 (2.503[a], 2.52[c])	9.00	1912	4.64	19.3	6.2
Nd	3.533	3.435×10^4	2.48 (2.488[a]; 2.49[b]; 2.48[c])	9.00 (9.5[b]; 8.9[d])	1482	4.63	19.2	6.4
Pm	3.603	3.054×10^4	2.44	8.97	642	4.60	19.2	7.5
Sm	3.617	2.975×10^4	2.42 (2.455[a])	8.94 (8.5[d])	425	4.60	19.1	7.0
Eu	3.630	2.912×10^4	2.41 (2.424[a]; 2.43[b]; 2.41[c])	8.90 (9.3[b])	245	4.58	19.0	7.6
Gd	3.643	2.851×10^4	2.39 (2.415[a])	8.72	254	4.55	18.9	7.8
Tb	3.656	2.791×10^4	2.37 (2.390[a])	8.59	171	4.55	18.9	7.2
Dy	3.667	2.723×10^4	2.36 (2.373[a]; 2.37[c])	8.36 (7.9[d])	226	4.52	18.7	8.0
Ho	3.681	2.686×10^4	2.34 (2.359[a])	8.24	246	4.52	18.6	8.0
Er	3.692	2.640×10^4	2.33 (2.340[a])	8.14	351	4.51	18.7	8.8
Tm	3.702	2.598×10^4	2.33 (2.334[a]; 2.32[c])	8.06	527	4.50	18.3	8.9
Yb	3.711	2.565×10^4	2.32 (2.317; 2.32[b])	8.02 (8.7[b]; 7.9[d])	665	4.49	18.3	9.2
Lu	3.719	2.527×10^4	2.32 (2.310[a])	8.01	1327	4.50	18.3	9.7

a: from Ref. [63]; b: from Ref. [61]; c: from Ref. [64]; d: from Ref. [65].

have used an empirical relationship

$$B_{\text{LnO}} = B_{\text{LaO}} + k \Delta r \qquad (4)$$

where Δr is the difference between La and Ln published ionic radius and k is a proportionality factor that was assumed to be $1 \, \text{Å}^{-2}$. This is ans assumption that is verified a posteriori comparing CLMD results with experimental data.

C parameters were determined such as the repulsion barriers of non-electrostatic curves for $La^{3+}\text{-OH}_2$ and $Ln^{3+}\text{-OH}_2$ are identical, once B are modified. Thus, since A is kept fixed, we adjusted C parameters to equalize the repulsion barriers. Paramaters used in the present calculations are presented in Table 4, while more details on the parametrization are given elsewhere [51, 52].

CLMD simulations of all the atoms in the Lanthanide series provide the correct behaviour in CN and La−O distances, as shown in the same Table 4. In particular we correctly reproduced the changing in coordination number through the series. For light Ln we have $\text{CN} = 9$ with the same structure obtained for La^{3+}, *i.e.* a tricapped trigonal prism (TTP) structure, while at the end we have $\text{CN} = 8$ structures that have a tridimensial arrangement that dynamically oscillate between a bicapped trigonal prism (BTP) and square antiprism (SAP) structure. We should note that in the middle of the series we do not get integer CN's which corresponds to having the interconversion between $\text{CN} = 9$ and $\text{CN} = 8$ during the 3 ns of simulation. Several exchange processes of water molecules in the first shell are observed, and the 3 ns are statistically enough to provide a correct picture of the relative probability between the two structures. As we have shown in details [68] molecular dynamics calculation were essential to show that the middle region of the series is characterized by a small mean residence time (MRT), as shown in the same Table 4. More details on structure and dynamics of lanthanide series hydration are reported elsewhere [52]. Here we focus our attention on MD *vs*. EXAFS comparison. A detailed analysis using the reconstruction of EXAFS signal by Eq. (2) is performed here

only for La^{3+}, while for other lanthanides it is a systematic work that need a specific study beyond the aim of the present study.

We should pause to make a consideration on polarization (α) and ionici radii (r_i) taken from experiments and used to modify the potential parameters B, C and α. They depend experimentally on the coordination number (CN) and we have arbitrarly choosen to use α and r_i corresponding to $\text{CN} = 9$ for lanthanides from Ce to Nd and those corresponding to $\text{CN} = 8$ for other Ln. This does not mean that CN is directly a parameter of the potential. Of course, since our question is to determine the CN and its behavior across the series, we had to make an arbitrarly choice a priori on which experimental α and r_i use, looking after for results. From what we have obtained we can say that: i) experimental data are correctly reproduced, thus giving a justification to parameters employed; ii) moreover the idea that each species has a unique CN in solution is what our studies have broken down [68], in agreement with recent experiments [69], thus strengthening the view that CN cannot be – even indirectly – a real parameter of our analytic potential.

Finally, as previously remarked for the choice of k in Eq. (4), our spirit is that we make some relatively arbitrary – but reasonable – assumption and then we verify these assumptions comparing our theoretical results with experimental data.

Note that our results are in good agreement with EXAFS data present in the literature. Our CLMD results can thus be used for a better EXAFS fitting. In particular, it is well known that coordination number is a very difficult parameter to fit, such that it is often fixed in EXAFS studies. The knowledge of coordination numbers issued from theoretical calculations can thus further improve the fitting of experimental data.

4. Conclusions

In this paper, we show how molecular dynamics and EXAFS experiments can be efficiently coupled to understand struc-

ture and dynamics of solvated metallic cations. In particular, both DFT-based and classical molecular dynamics can be successfully employed at this aim. In the case of strongly bound metal-water systems, where exchange reactions are negligible and only one mean structure is present in solution, DFT-based MD, that is limited to few picosecond length, can be employed. Classical MD can be used when exchange reactions and co-existence of different structures, interconverting in ps-ns time scale, take place, paying the price of a pre-parametrization work to correctly describe metal-water interactions.

DFT-based MD at the present time suffers the limitation of a limited available simulation time length (few ps) and the fact that only simple functionals (here BLYP) can be employed. This is reflected in a redshift of vibrational and related properties, such as overestimation of Debye–Waller factors or more generally a broader metal-water radial distribution function. Classical MD, on the other hand, simulating systems on the ns time scale, are able to describe water exchange reactions and to identify structures with different coordination number that interexchange in a ps-ns time scale. These simulations provide quite narrow distribution function as a quite general rule (as found also in other cases [37]), and metal-water distances that in our case are sistematically smaller than experiments, but with a very small discrepancy with experiments. However, these results can only be obtained after a careful parametrization of metal-water force fields.

The key result that we show here is that radial distribution functions obtained from simulations can be used in EXAFS signal reconstruction, obtaining results that are comparable with those previously known. Simulations can be used thus in several steps of the EXAFS data analysis: (i) structures picked from MD simulations can be used as reference structure to calculate phase shifts; (ii) coordination numbers, that are the most sensitive parameter in EXAFS fitting, can be obtained from simulations and kept fixed in the fitting; (iii) metal-water radial distribution functions obtained from simulations can be used directly in the EXAFS data fitting. We have presented here that different molecular dynamics methods and different hydration structures (octahedric and trigonal tricapped prism, TTP) can both well reproduce EXAFS signals.

Finally, we have shown that a classical potential parametrized from the first atom of a series (here the lanthanide series) can be extended to the whole series, when ions are at the same oxidation state, without an hard reparameterization work but just using physical atomic properties available, obtaining results with the same quality as for the initial atom, for which the classical potential parameters are parameterized with high level *ab initio* calculations. This can be very useful to study a whole class of elements, like actinides, for which *ab initio* dynamics for all the atoms in the series are computationally prohibitive. As a result, the structure and dynamics around metal cations can be studied also when it is experimentally difficult, as for lanthanides in extreme conditions or radioactive actinides. Note that, since lanthanides(III) are the chemical analogue of actinide(III), the solvation trends here obtained can be also inferred for hydration of trivalent actinides.

References

1. Helm, L., Merbach, A. E.: Inorganic and bioinorganic solvent exchange mechanisms. Chem. Rev. **105**, 1923–1959 (2005).
2. Ohtaki, H., Radnai, T: Structure and dynamics of hydrated ions. Chem. Rev. **93** 1157–1204 (1993.
3. Marcus, Y.: Ionic radii in aqueous solutions. Chem. Rev. **88**, 1475–1498 (1988).
4. Johansson, G.: Structures of complexes in solution derived from X-ray diffraction measurements. Adv. Inorg. Chem. **39**, 159–232 (1992).
5. Rotzinger, F. P.: Treatement of substitution and rearrangement mechanisms of transition metal complexes with quantum chemical methods. Chem. Rev. **105**, 2003–2038 (2005).
6. Aakesson, R., Petterson, L. G. M., Sandstroem, M., Wahlgren, U.: Ligand field effects in the hydrated divalent and trivalent metal ions of the first and second transition periods. J. Am. Chem. Soc. **116**, 8691–8704 (1994).
7. Siboulet, B., Marsden, C. J., Vitorge, P.: A theoretical study of uranyl solvation: explicit modelling of the second hydration sphere by quantum mechanical methods. Chem. Phys. Lett. **326**, 289–296 (2006).
8. Martinez, J. M., Pappalardo, R. R., Sanchez Marcos, E.: Study of Ag^+ hydration by means of a semicontinuum quantum-chemical solvation model. J. Phys. Chem. A **101**, 4444–4448 (1997).
9. Martinez, J. M., Pappalardo, R. R., Sanchez Marcos, E., Mennucci, B., Tomasi, J.: Analysis of the opposite solvent effects caused by different solute cavities on the metal-water distance of monoatomic cation hydrates. J. Phys. Chem. B **106**, 1118–1123 (2002).
10. Sprik, M., Hutter, J., Parrinello, M.: *Ab initio* molecular dynamics simulation of liquid water: Comparison of three gradient-corrected density functional. J. Chem. Phys. **105** 1142–1152 (1996).
11. Sokolic, F., Guissani, Y., Guillot, B.: Computer simulation of liquid sulphur dioxide: comparaison of model potentials. J. Phys. Chem. **89**, 3023–3026 (1985).
12. Rey, R., Hynes, J. T.: Hydration shell exchange kinetics: an MD study for Na^+. J. Phys. Chem. **100**, 5611–5615 (1996).
13. D'Alessandro, M., D'Abramo, M., Brancato, G., Di Nola, A., Amadei, A.: Statistical mechanics and thermodynamics of simulated ionic solutions. J. Phys. Chem. B **106**, 11843–11848 (2002).
14. Chillemi, G., Mancini, G., Sanna, N., Barone, V., Della Longa, S., Benfatto, M., Pavel, N. V., D'Angelo, P.: Evidence for sevenfold coordination in the first solvation shell of Hg(II) aqua ion. J. Am. Chem. Soc. **129**, 5430–5436 (2007).
15. Simon, C., Cartailler, T., Turq, P.: Structure and speciation of liquid 2HF/KF: a molecular dynamics study. J. Chem. Phys. **117**, 3772–3779 (2002).
16. Eichkom, K., Weigend, F., Treutler, O., Ahlrichs, R.: Auxiliary basis sets for main row atoms and transition metals and their use to approximate Coulomb potentials. Theor. Chem. Acc. **97**, 119–124 (1997).
17. Hafner, P., Schwarz, W. H. E.: Pseudo-potential approach including relativistic effects. J. Phys. B At. Mol. Phys. **11**, 217–233 (1978).
18. Dang, L. X., Schenter, G. K., Fulton, J. L.: EXAFS spectra of the diluite solutions of Ca^{2+} and Sr^{2+} in water and methanol. J. Phys. Chem. B **107**, 14119–14123 (2003).
19. Amadei, A., Aschi, M., Spezia, R., Di Nola, A.: A first principles polarizable water model for molecular simulations: application to a water dimer. J. Mol. Liq. **101**, 181–198 (2002).
20. Duvail, M., Souaille, M., Spezia, R., Cartailler, T., Vitorge, P.: Pair interaction potentials with explicit polarization for molecular dynamics simulations of La^{3+} in bulk water. J. Chem. Phys. **127**, 034503 (2007).

21. Yazyev, O. V., Helm, L.: Gadolinium(III) ion in liquid water: Structure, dynamics, and magnetic interactions from first principles. J. Chem. Phys. **127**, 084 506 (2007).

22. Buhl, M., Grigoleit, S., Kabrede, H., Mauschick, F. T.: Simulation of ^{59}Co NMR chemical shifts in aqueous solution. Chem. Eur. J. **121**, 477–488 (2006).

23. Yazyev, O. V., Helm, L.: Hyperfine interactions in aqueous solution of Cr^{3+}: an *ab initio* molecular dynamics study. Theor. Chem. Acc. **115**, 190–195 (2006).

24. Amira, S., Spangberg, D., Zelin, V., Probst, M., Hermansson, K.: Car-Parrinello molecular dynamics simulation of Fe^{3+} (aq). J. Phys. Chem. B **109**, 14 235–14 242 (2005).

25. Vuilleumier, R., Sprik, M.: Electronic properties of hard and soft ions in solution: Aqueous Na$^+$ and Ag$^+$ compared. J. Chem. Phys. **115**, 3454–3468 (2001).

26. Spezia, R., Nicolas, C., Boutin, A., Vuilleumier, R.: Molecular dynamics simulations of a silver atom in water: evidence of a dipolar excitonic state. Phys. Rev. Lett. **91**, 208 304 (2003).

27. Ensing, B., Baerends, E.: Reaction path sampling of the reaction between iron(II) and hydrogen peroxide in aqueous solution. J. Phys. Chem. A **106**, 7902–7910 (2002).

28. Pasquarello, A., Petri, I., Salomon, P. S., Parisel, O., Car, R., Toth, E., Powell, D. H., Fischer, H. E., Helm, L., Merbach, A. E.: First solvation shell of the Cu(II) aqua ion: evidence for fivefold coordination. Science **291**, 856–859 (2001).

29. Lubin, M. I., Bylaska, E. J., Weare, J. H.: *Ab initio* molecular dynamics simulations of aluminium ion solvation in water clusters. Chem. Phys. Lett. **322**, 447–453 (2000).

30. Marx, D., Sprik, M., Parrinello, M.: *Ab initio* molecular dynamics of ion solvation. The case of Be^{2+} in water. Chem. Phys. Lett. **273**, 360–366 (1997).

31. D'Angelo, P., Di Nola, A., Filipponi, A., Pavel, N. V., Roccatano, D.: An extended X-ray absorption fine structure study of aqueous solutions by employing molecular dynamics simulations. J. Chem. Phys. **100**, 985–994 (1994).

32. Roccatano, D., Berendsen, H. J. C., D'Angelo, P.: Assessment of the validity of intermolecular potential models used in molecular dynamics simulations by extended X-ray absorption fine structure spectroscopy: A case study of Sr^{2+} in methanol solution. J. Chem. Phys. **108**, 9487–9497 (1998).

33. D'Angelo, P., Barone, V., Chillemi, G., Sanna, N., Meyer-Klaucke, W., Pavel, N. V.: Hydrogen and higher shell contributions in Zn^{2+}, Ni^{2+} and Co^{2+} aqueous solutions: An X-ray absorption fine structure and molecular dynamics study. J. Am. Chem. Soc. **124**, 1958–1967 (2002).

34. D'Angelo, P., Chillemi, G., Barone, V., Mancini, G., Sanna, N., Persson, I.: Experimental evidence for a variable first coordination shell of the cadmium(II) ion in aqueous, dimethyl sulfoxide, and N,N'-dimethylpropyleneurea solution. J. Phys. Chem. B **109**, 9178–9185 (2005).

35. Ferlat, G., Soetens, J., San Miguel, A., Bopp, P. A.: Combining extended x-ray absorption fine structure with numerical simulations for disordered systems. J. Phys. Condens. Matter **17**, S145–S157 (2005).

36. Ferlat, G., San Miguel, A., Xu, H., Aouizerat, A., Blase, X., Zuniga, J., Munoz-Sanjosé, V.: Semiconductor-metal transitions in liquid In$_{100-x}$Se$_x$ alloys: A concentration-induced transition. Phys. Rev. B **69**, 155 202 (2004).

37. Spezia, R., Duvail, M., Vitorge, P., Cartailler, T., Tortajada, J., Chillemi, G., D'Angelo, P., Gaigeot, M.-P.: A coupled Car-Parrinello molecular dynamics and EXAFS data analysis investigation of aqueous Co^{2+}. J. Phys. Chem. A **110**, 13 081–13 088 (2006).

38. Poiarkova, A. V., Rehr, J. J.: Multiple-scattering X-ray-absorption fine-structure Debye–Waller factor calculations. Phys. Rev. B **59**, 948–957 (1999).

39. Dang, L. X., Schenter, G. K., Glezakou, V.-A., Fulton, J. L.: Molecular simulation analysis and X-ray absorption measurement of Ca^{2+}, K$^+$, Cl$^-$ ions in solution. J. Phys. Chem. B **110**, 23 644–23 654 (2006).

40. Van Hung, N., Rehr, J. J.: Anharmonic correlated Einstein-model Debye–Waller factors. Phys. Rev. B **56**, 43–46 (1997).

41. Rehr, J. J., Albers, R. C.: Theoretical approaches to X-ray absorption fine structure. Rev. Mod. Phys. **72**, 621–654 (2000).

42. Car, R., Parrinello, M.: Unified approach for molecular dynamics and density-functional theory. Phys. Rev. Lett. **55**, 2471–2474 (1985).

43. Hutter, J., Alavi, A., Deutsch, T., Bernasconi, M., Goedecker, S., Marx, D., Tuckerman, M., Parrinello, M. CPMD version 3.7.2. IBM Research Division, IBM Corp. and Max Planck Institut-Stuttgart.

44. Trouillier, N., Martins, J. L.: Efficient pseudopotential for plane-wave calculations. Phys. Rev. B **43**, 1993–2006 (1991).

45. Cotton, F. A., Wilkinson, G.: *Advanced Inorganic Chemistry*. Wiley, New York (1980).

46. Bresson, C., Spezia, R., Esnouf, S., Solari, P. L., Coantic, S., Den Auwer, C.: A combined spectroscopic and theoretical approach to investigate structural properties of Co(II)/Co(III) tris-cysteinato complexes in aqueous medium. New J. Chem. **31**, 1789–1797 (2007).

47. Spezia, R., Tournois, G., Tortajada, J., Cartailler, T., Gaigeot, M.-P.: Toward a DFT-based molecular dynamics description of Co(II) binding in sulfur-rich peptides. Phys. Chem. Chem. Phys. **8**, 2040–2050 (2006).

48. Kleinman, L., Bylander, D. M.: Efficacious form for model pseudopotentials. Phys. Rev. Lett. **48**, 1425–1428 (1982).

49. Louie, S. G., Froyen, S., Cohen, M. L.: Nonlinear ionic pseudopotentials in spin-density-functional calculations. Phys. Rev. B **26**, 1738–1742 (1982).

50. Jorgensen, W. L., Chandrasekhar, J., Madura, J. D., Impey, R. W., Klein, M. L.: Comparison of simple potential functions for simulating liquid water. J. Chem. Phys. **79**, 926–935 (1983).

51. Duvail, M.: Etude des trications lanthanide en solution aqueouse par dynamique moléculaire. PhD Thesis, Université Paris XI (2007).

52. Duvail, M., Vitorge, V., Spezia, R.: Building a polarizable pair interaction potential for lanthanoids(III) in liquid water: A molecular dynamics study of structure and dynamics of the whole series. J. Chem. Phys. **130**, 104 501 (2009).

53. Thole, B. T.: Molecular polarizabilities calculated with a modified dipole interaction. Chem. Phys. **59**, 341–350 (1981).

54. Sprik, M.: Computer simulation of the dynamics of induced polarization fluctuations in water. J. Phys. Chem. **95**, 2283–2291 (1991).

55. Filipponi, A., Di Cicco, A., Natoli, C.: X-ray-absorption spectroscopy and *n*-body distribution functions in condesed matter. I. Theory. Phys. Rev. B **52**, 15 122–15 134 (1995).

56. Filipponi, A., D'Angelo, P., Pavel, N. V., Di Cicco, A.: Triplet correlations in the hydration shell of aquaions. Chem. Phys. Lett. **225**, 150–155 (1994).

57. Hedin, L., Lundqvist, B. I.: Explicit local exchange-correlation potentials. J. Phys. C **4** 2064–2083 (1971).

58. Krause, M. O., Oliver, J. H.: Natural widths of atomic *K* and *L* levels, K_α X-ray lines and several *KLL* Auger lines. J. Phys. Chem. Ref. Data **8**, 329–338 (1979).

59. Filipponi, A., Borowski, M., Bowron, D. T., Ansell, S., Di Cicco, A., De Panfilis, S.: An experimental station for advanced research on condensed matter under extreme conditions at the European Synchrotron Radiation Facility – BM29 beamline. Rev. Sci. Instrum. **71**, 2422–2432 (2000).

60. D'Angelo, P., De Panfilis, S. , Filipponi, A., Persson, I.: High-energy X-ray absorption spectroscopy: a new tool for structural investigations of lanthanoids and third row transition elements. Chem. Eur. J. **14**, 3045–3055 (2008).

61. Allen, P., Bucher, J. J., Shuh, D. K., Edelstein, N. M., Craig, I.: Coordination chemistry of trivalent lanthanide and actinide ions in dilute and concentrated chloride solutions. Inorg. Chem. **39**, 595–601 (2000).

62. Naslund, J., Lindqvist-Reis, P., Persson, I., Sandstrom, M.: Inorg. Chem. **39**, 4006–4011 (2000).

63. Ishiguro, S.-I, Umebayashi, Y., Kato, K., Takahashib, R., Ozutsumic, K.: Strong and weak solvation steric effects on lanthanoid(III) ions in N,N-dimethylformamide-N,N-dimethylacetamide mixtures. J. Chem. Soc. Faraday Trans. **94**, 3607–3612 (1998).

64. Solera, J. A., Garcia, J., Proietti, M. G.: Multielectron excitations at the *L* edges in rare-earth ionic aqueous solutions. Phys. Rev. B **51**, 2678–2686 (1995).

65. Helm, L., Merbach, A. E.: Structure and dynamics of lanthanide(III) ions in solution: a neutron scattering contribution. Eur. J. Solid Inorg. Chem. **28**, 245–250 (1991).
66. Shannon, R. D.: Revised effective ionic radii and systematic studies of interatomic distances in halides and chalcogenides. Acta Crist. A **32**, 751–767 (1976).
67. Lide, D. R. (ed.): *Handbook of Physics and Chemistry*. CRC Press, Boca Raton, FL (1996).
68. Duvail, M., Spezia, R., Vitorge, V.: A dynamic model to explain hydration behaviour along the Lanthanide series. Chem. Phys. Chem. **9**, 693–696 (2008).
69. Persson, I., D'Angelo, P., De Panfilis, S., Sandstom, M., Eriksson, L.: Hydratin of lanthanoid(III) ions in aqueous solution and crystalline hydrates by EXAFS spectroscopy and crystallography: the myth of the "Gadolinium Break". Chem. Eur. J. **14**, 3056–3066 (2008).